Journal of Hydrology 616 (2023) 128823

Contents lists available at ScienceDirect

Journal of Hydrology

journal homepage: www.elsevier.com/locate/jhydrol

Research papers

Data analysis and integrated modeling of compound flooding impacts on coastal drainage infrastructure under a changing climate

Yousef Sangsefidi [a,b,*], Kian Bagheri [a,b], Hassan Davani [b], Mark Merrifield [c]

[a] Department of Mechanical and Aerospace Engineering, University of California–San Diego (UCSD), CA, USA
[b] Department of Civil, Construction, and Environmental Engineering, San Diego State University (SDSU), CA, USA
[c] Scripps Institution of Oceanography, University of California–San Diego (UCSD), CA, USA

ARTICLE INFO

This manuscript was handled by Emmanouil Anagnostou, Editor-in-Chief, with the assistance of Giulia Sofia, Associate Editor

Keywords:
Climate change
Sea-level rise
Coastal areas
Compound flooding
Groundwater infiltration
Stormdrain system

ABSTRACT

Low-lying coastal areas are susceptible to multiple types of flooding from marine, subsurface, and surface sources. The co-occurrence of a rainfall event with high sea level, which raises coastal groundwater tables conjointly, may result in a compound flooding event, which could be much more widespread and dangerous than that of an individual flooding source. Focusing on Imperial Beach as a low-elevation coastal community in California, this paper provides a generalized methodology to determine the vulnerability of coastal stormdrain systems to compound seawater, groundwater, and stormwater flooding under a changing climate. Although marine inundation by itself is expected to flood only 7% of the study area by 2100 under the most pessimistic scenario (i.e. 2 m rise), our results show that more than 20% of the study area's subterranean stormdrain system is already at the risk of subsurface flooding at current sea levels. While marine inundation is a concern near the coastline as sea level rises, the results show that seawater intrusion into the stormdrain system can impact areas kilometers away from the coastline. The consequences of sea-level rise (SLR) can be exacerbated by an under-resourced stormdrain system, caused by groundwater infiltration through system defects. As such, by a 2 m rise in current sea-level, the flooding volume may double in an ideal system (i.e., no defects) while this ratio can increase six fold in a slightly defective stormdrain system (with 0.25 % porosity systemwide). The continuous simulations of the stormdrain system performance indicate that flood events will be more destructive and frequent under these circumstances.

1. Introduction

Global warming, attributed to greenhouse gas emissions, is changing the natural water cycle on the earth. In the wake of melting glaciers and ice sheets as well as thermal expansion of ocean water, the global mean sea level has increased at a rate of ~3.1 mm/year since the mid-1990s (Sweet et al., 2022), which is faster than any equivalent period over at least the last 2700 years (Kopp et al., 2016). Depending on future emissions, the continental US coastline is projected to see 0.6–2.2 m of Sea-Level Rise (SLR) at the end of the century (Sweet et al., 2022). Climate projections also raise concerns about how precipitation will respond in a warming world. While longer droughts are expected in most regions due to rising temperatures (attributed to higher surface evaporation), global models project a 16–24 % increase in heavy precipitation intensity by 2100 (associated with larger water-holding capacity of the warmer air) (Fischer et al., 2014; Trenberth, 2011). As shown in Fig. 1, due to the interactions of oceanographic, hydrological, and meteorological processes, low-lying coastal areas are susceptible to different sources of marine, subsurface, and surface inundation, especially after considering climate change effects on water resources (Befus et al.,

Abbreviations: A_{eff}, effective area of a conduit for groundwater infiltration (m^2); C1, C2, C3, and C4 abbreviations used for specifying conduits; C_d, discharge coefficient of a circular orifice; D, circular conduit diameter (m); d, circular defect diameter (m); EL_d, rim elevation of the downstream node of a conduit (m); EL_u, rim elevation of the upstream node of a conduit (m); GWI, GroundWater Infiltration (m^3/s); GWI_i, GWI in the presence of SWI (m^3/s); GWI_j, GWI in the absence of SWI (m^3/s); GWI_k, GWI in the absence of SWI when GWT = sea level (m^3/s); GWT, GroundWater Table (m); GWT_{ave}, average GWT on a conduit (m); g, gravity acceleration (≈ 9.81 m/s^2); H_G, groundwater head on a conduit (m); K, hydraulic conductivity (m/day); L, conduit length (m); L_{eff}, effective length of a conduit for groundwater infiltration (m); LECZ, Low-Elevation Coastal Zone; MI, Marine Inundation; N, number of defects; P, system porosity (%); Q_d, groundwater infiltration rate through a single defect (m^3/s); R, hydraulic radius of a non-circular conduit (m); SLR, Sea-Level Rise (m); SWI, SeaWater Intrusion (m^3/s); ε, soil void ratio.

* Corresponding author at: Department of Mechanical and Aerospace Engineering, University of California–San Diego (UCSD), CA, USA.
E-mail address: ysangsefidi@ucsd.edu (Y. Sangsefidi).

https://doi.org/10.1016/j.jhydrol.2022.128823
Received 12 March 2022; Received in revised form 12 August 2022; Accepted 9 November 2022
Available online 26 November 2022

2020; Bevacqua et al., 2019). Thus, efficient management of coastal drainage systems requires new information about the current and future role of seawater and groundwater sources along with the typical stormwater source in urban flooding.

Currently, over 20 million people of the world's population are permanently exposed to marine inundation while more than 200 million people are vulnerable to marine flooding during temporary extreme high sea-level events (Nicholls, 2011). SLR will enhance coastal marine inundation (Zone I in Fig. 1), which has been projected to impact ~13 million people directly in the United States by 2100 [assuming 1.8 m of SLR, Hauer et al. (2016)]. SLR also will magnify the impacts of extreme sea-level events as their frequency and magnitude follow a sharply escalating pattern (Thompson et al., 2021; Vitousek et al., 2017). According to Kirezci et al. (2020), for a 1-meter SLR scenario at the end of the current century, there will be a ~50 % increase in the global population, assets, and land area at risk of seawater flooding. The projected SLR will dramatically threaten coastal communities and ecosystems such that it may shift the coastline landward, accelerate cliff failure and beach erosion, degrade coastal habitats and aquifers, and potentially damage coastal infrastructure (Arkema et al., 2013; Dawson et al., 2009; Nicholls and Cazenave, 2010; Rotzoll and Fletcher, 2013).

While flood control measures typically are designed to protect coastal communities from seawater flooding, there is growing recognition that Low-Elevation Coastal Zones (LECZ: coastal areas below 10 m of elevation above sea level) also are vulnerable to subsurface flooding (Zone II in Fig. 1) (Befus et al., 2020). Coastal groundwater tables are dynamically connected to sea levels, and thus their inland responses to SLR, known as groundwater emergence and shoaling, may pose a further threat to terrestrial infrastructure and natural resources (Hoover et al., 2017; Sukop et al., 2018). By modeling groundwater flow in a dense urban site along the Hudson River Estuary in New Jersey, Su et al. (2022) predicted that for SLR up to 1 m, one third of the study area would be impacted by subsurface flooding. Across urbanized coastal zones, shallow groundwater (i.e., <2 m depth) also may immerse subterranean infrastructures (e.g., drainage and sewer networks, electric and gas substations, building foundations) and cause serious disruptions to their operation, maintenance and development (Habel et al., 2020; Rotzoll and Fletcher, 2013). Besides intensifying chemical corrosion and deterioration, high-level groundwater can intrude into water conveyance networks through their defects (e.g., holes, cracks, and misaligned joints) and increase their hydraulic loading (Dirckx et al., 2016; Karpf and Krebs, 2011; Su et al., 2022). Previous studies indicate that groundwater infiltration into sewer systems ranges from 30 to 72 % of total sewage flow (Zhao et al., 2020), which may triple in LECZs with 1 m SLR (Fung and Babcock, 2020). Compared to soil type and sewer pipe characteristics, the groundwater table is the most important parameter affecting groundwater infiltration in LECZs (Liu et al., 2021).

Considering rainfall events and subsequent stormwater runoff as a key source of inundation (Zone III in Fig. 1), LECZs are critically exposed to compound flooding where multiple flooding pathways co-occur (Jang and Chang, 2022; Rahimi et al., 2020). Through compound events when heavy precipitation coincides with an extreme sea-level event, the flooding extent substantially increases compared to that of either in isolation (Moftakhari et al., 2019; Saharia et al., 2021; Wahl et al., 2015). For example, by coupling heavy rainfall and high sea-level events, around 80 % of The City of New Orleans in the United States was inundated for several weeks in 2005 (Moghimi et al., 2021). The vulnerability of coastal communities to compound flooding is expected to critically exacerbate over the century due to SLR and climate change effects on heavy rainfall patterns, which lead to further reductions in terrestrial infiltration, ponding, and drainage capacity (Davtalab et al., 2020; Karamouz et al., 2015).

In recent years, enhanced awareness of the potentially catastrophic impacts of compound flooding on human lives and property has motivated new assessments of the multiple and interconnected drivers of compound flooding in different natural and urbanized areas. Table 1 presents a summary of recent selected studies on compound flooding. Using MIKE Urban 1D model and focusing on the number of flooded junctions and flood frequency, Laster Grip et al. (2021) simulated the performance of a coastal stormdrain system under coupled events of SLR, storm surge, and rainfall. While the model was neither calibrated nor validated, their comparative studies reported that although the impact of SLR is not evident today, a tipping point will occur in 2075–2100, after which storm surges become a major driver for stormdrain system failure. While rainfall-induced stormwater flooding was not included in the studies of Gold et al. (2022) and Habel et al. (2020), their evaluation of stormdrain system performance under high tides showed that the system may flood due to seawater backflow (even in the absence of precipitation). By studying coupled storm surge and rainfall events, Tahvildari et al. (2022) and Khanam et al. (2021)

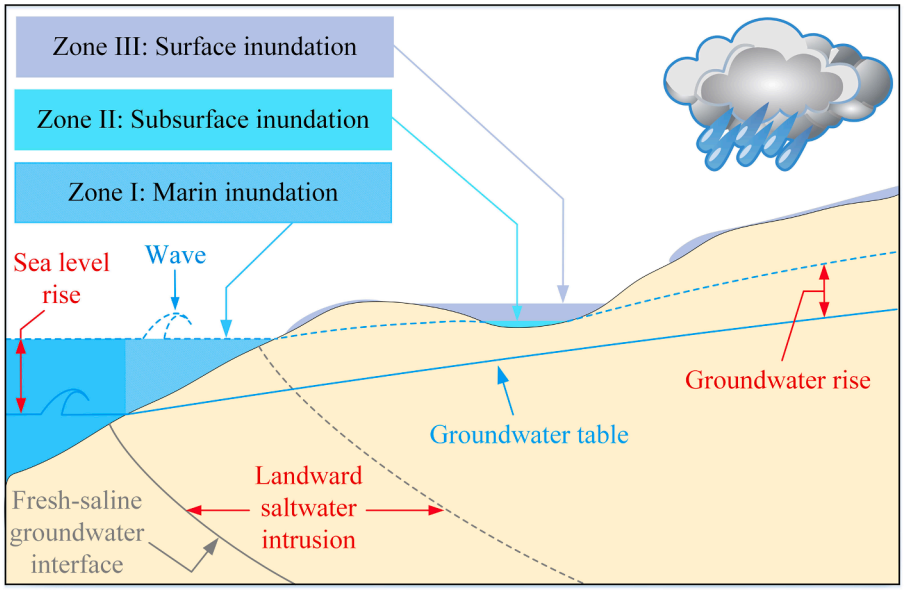

Fig. 1. Schematic view of different sources of inundation along with sea level, groundwater table, and fresh-saline groundwater interface for current (solid line) and future (dashed line) conditions.

Table 1
Summary of conducted studies on compound flooding in recent years.

Study	Case Study	Flooding component	Main insight
Laster Grip et al. (2021)	Stormdrain system (Trelleborg, Sweden)	Storm surge, SLR, and rainfall	Dominance of storm surges for drainage flooding frequency in the last quarter of this century
Gold et al. (2022)	Stormdrain system (Beaufort, Wilmington, New Bern, and Nags Head, NC, USA)	High tide	Stormdrain backflow flooding in the absence of precipitation
Habel et al. (2020)	Stormdrain system (Honolulu, HI, USA)		
Tahvildari et al. (2022)	Roadway networks (Hampton Roads, VA, USA)	Storm surge and rainfall	Larger flooding extent as a measure of the potential threat to urban infrastructure systems
Khanam et al. (2021)	Electric infrastructure (Connecticut, CT, USA)	Storm surge, SLR, and rainfall	
Davtalab et al. (2020)	Stormwater retention pond (Tampa Bay, FL, USA)	SLR-driven groundwater rise	Poor performance of retention pond due to the infiltration reduction
Rahimi et al. (2020)	Riverine stream (Oakland Flatlands, CA, USA)	SLR-driven groundwater rise and rainfall	Larger extent of river flooding due to reduction in its discharge capacity

quantified the flooding extent as a measure of the potential threat to roadway networks and electric infrastructure during compound events. Davtalab et al. (2020) and Rahimi et al. (2020) reported higher risks of flooding in retention ponds and riverine streams during SLR-induced groundwater rise associated with the reduction in their infiltration and discharge capacity, respectively.

Although the previous studies (listed in Table 1) confirm the vulnerability of coastal communities to compound flooding events, due to the multiplicity and complexity of involved mechanisms, additional research is needed to quantify compound flooding risk and subsequently establish efficient adaptation strategies for mitigating climate change stresses on water infrastructures. This study develops a novel and general framework to assess the vulnerability of coastal stormdrain systems to compound mechanisms of seawater, groundwater, and stormwater flooding under emerging climate change scenarios. We focus on a case study of Imperial Beach (IB), which is a coastal community in California surrounded by water bodies on three sides and vulnerable to compound flooding [Fig. 2(a)]. Different sources of marine, subsurface, and surface inundations (shown in Fig. 1) are evaluated using a 'bathtub' approach, the MODFLOW groundwater model developed by Befus et al. (2020), and the integrated hydrology-hydraulic PCSWWM model developed for this study. ArcGIS is utilized for geospatial analysis and flood mapping. The principal objectives of this study are to:

- identify the extent and volume of seawater intrusion and groundwater infiltration into coastal stormdrain systems by studying different scenarios for SLR, hydraulic conductivity, and system defects;
- advance knowledge on the vulnerability of coastal drainage infrastructure to coupled oceanographic, hydrological, and meteorological stressors; and
- examine climate change impacts (i.e., SLR, groundwater rise, and more intense rainfall) on the performance of coastal stormdrain systems through estimating the extent and frequency of flood events.

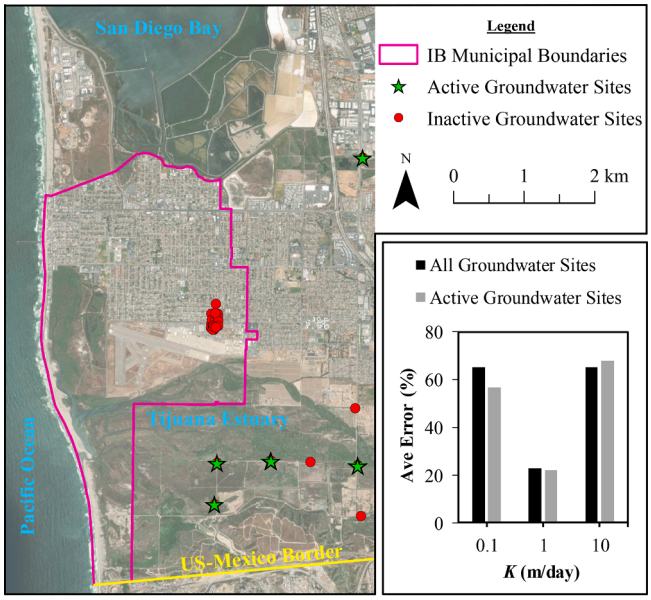

(a) (b)

Fig. 2. Demonstration of (a) Imperial Beach situation to the surrounding water bodies and nearby groundwater sites and (b) the difference between the observed and modeled groundwater table data.

2. Material and methods

2.1. Study area

Imperial Beach (IB) is the southwestern-most city in the continental United States with ~ 30 thousand population, ~5.5 km^2 area, ~2.5 km coastline, and 2–10 m elevation (Gallien, 2016). As a LECZ, the residential area of this underserved community is surrounded by water bodies from three sides: The Pacific Ocean on the west, San Diego Bay on the north, and Tijuana Estuary on the south [Fig. 2(a)]. Due to its unique setting and aged water infrastructure, IB is vulnerable to compound flooding, particularly when a rainfall event occurs while the stormdrain system is significantly occupied by SeaWater Intrusion (SWI) and/or GroundWater Infiltration (GWI).

Table 2
Description of the main datasets used in the current study.

Data		Source	Description
Digital Elevation Model (DEM)		SANDAG ArcGIS Server	Resolution: 0.762 m × 0.762 m
Sea level (SL)		NOAA–Tides and Currents	SL = 1.658, 2.658, and 3.658 m for SLR = 0, 1 and 2 m at MHHW
Groundwater table	Modeled spatial data	Befus et al. (2020)–MODFLOW model	Resolution: 10 m × 10 m; K = 0.1, 1, 10 m/d; Datum: MHHW& LMSL
	Observed data point	USGS–National Water Information System	No active groundwater site inside IB
Stormdrain system data		City of Imperial Beach	Conducting multiple field visits to fill missing data
Rainfall data	Nested Storm	NOAA Atlas SD Hydro Tools	Converting NOAA's precipitation-frequency data to 24-hr nested storm using the SD Hydro Tools package
	Historical data	Project Clean Water	Considering 1983–1986 water years as the representative wet period

2.2. Primary datasets

Table 2 describes the main datasets obtained and utilized in this study. Topographic data is acquired from a high-resolution Digital Elevation Model (DEM with 0.762 m × 0.762 m resolution) provided by the San Diego Association of Governments (SANDAG). The sea-level records are obtained from the National Oceanic and Atmospheric Administration (NOAA) for the San Diego Bay station (ID: 9410170), which is the closest tide station to the study area (located ~ 20 km north of IB with over a 100-year record). Following NOAA's regional SLR scenarios, we examine SLR = 0, 1, and 2 m. The scenario of SLR = 0 m refers to the present-day sea level at Mean Higher-High Water [MHHW = 1.658 m referenced to the North American Vertical Datum of 1988 (NAVD88)] while 1 and 2 m represent intermediate and high scenarios of SLR by 2100, associated with moderate and high greenhouse-gas emission scenarios over the century (Sweet et al., 2022). MHHW is obtained for the most recent 19 years (2002–2021) providing an estimation of high-water levels that are persistently and frequently reached in the region (Hoover et al., 2017).

Groundwater flow is generally described by Darcy's Law, which can be combined with conservation of mass to obtain a partial-differential equation describing the distribution of hydraulic head as the target parameter (Langevin et al., 2017). In this research, GroundWater Table (GWT) data is acquired and analyzed from the MODFLOW model developed by Befus et al. (2020). These researchers assessed the steady-state and three-dimensional responses of GWT to various SLR scenarios across the California coast (including IB) for three values of hydraulic conductivity (K = 0.1, 1, and 10 m/day). To validate the applicability of MODFLOW results for IB, we have compared the modeled GWT at Local Mean Sea Level (LMSL) with temporal mean values of the observed GWT in nearby groundwater sites [available on the United States Geological Survey (USGS) website]. The best agreement between modeled and observed time-averaged GWT (within 20 %) is found for K = 1 m/d (Fig. 2). Thus, to obtain the spatial distribution of GWT across IB, the present study has utilized the MODFLOW data for K = 1 m/day and the mentioned SLR scenarios in Table 2.

The primary input parameters for the stormwater model (PCSWMM described below in section 2.3.3. Stormwater modeling) include stormdrain system specifications, rainfall and evaporation data, soil properties, and land-use characteristics. The spatial and geometric specifications of the stormdrain system elements (i.e., conduits, junctions, and outfalls) are available at the data warehouse of the City of IB (www.imperialbeachca.gov/stormwater). Gaps in the data have been filled through contacting the Environmental & Natural Resources Department in IB and conducting in-situ and virtual field visits by our research team and Google Street View. The hydrological package of SD Hydro Tools developed by The County of San Diego is utilized to generate 24-hr nested design storms (having 1-year, 2-year, and 100-year return periods) from NOAA's precipitation-frequency data. The design storms with 1-year and 2-year return periods represent heavy rainfall events while extreme rainfall events are represented by 100-year return period (occurring on average once in a century). In addition, 38 years of rainfall data with a 1-hour interval are obtained from Project Clean Water (www.projectcleanwater.org) to perform a continuous simulation of the stormdrain system performance. From Fig. 3, the time interval of 1983–1986 water years (with the maximum yearly, monthly, daily, and hourly values of 531, 198, 76, and 28 mm) is considered as the representative wet period and imported in the model. Other involved parameters in stormwater modeling (i.e., subcatchment roughness, imperviousness, and infiltration in addition to conduit roughness and energy loss) are set by referring to local sources covering the study area [e.g., The City of San Diego Stormwater Standards (2021) and County of San Diego Hydrology Manual (2003)]. These parameters are described in the section 2.3.3.

2.3. Methods

2.3.1. Marine and subsurface inundations

Fig. 4 presents the workflow carried out in the present study steps. The first studied component is Marin Inundation (MI), which represents the passive flooding from seawater across the coastline at MHHW level (as shown in Fig. 5(a) and described in section 3.1). Other sea-related flooding sources, like storm surge and wave runup, are not included in MI due to the focus of this research on the inland drainage system. The vulnerable locations to MI are identified using a bathtub approach in ArcGIS, which subtracts the sea-level elevation in a given scenario from the DEM to identify the areas that host elevations below that of the seawater surface (Habel et al., 2020). Due to topographic obstructions,

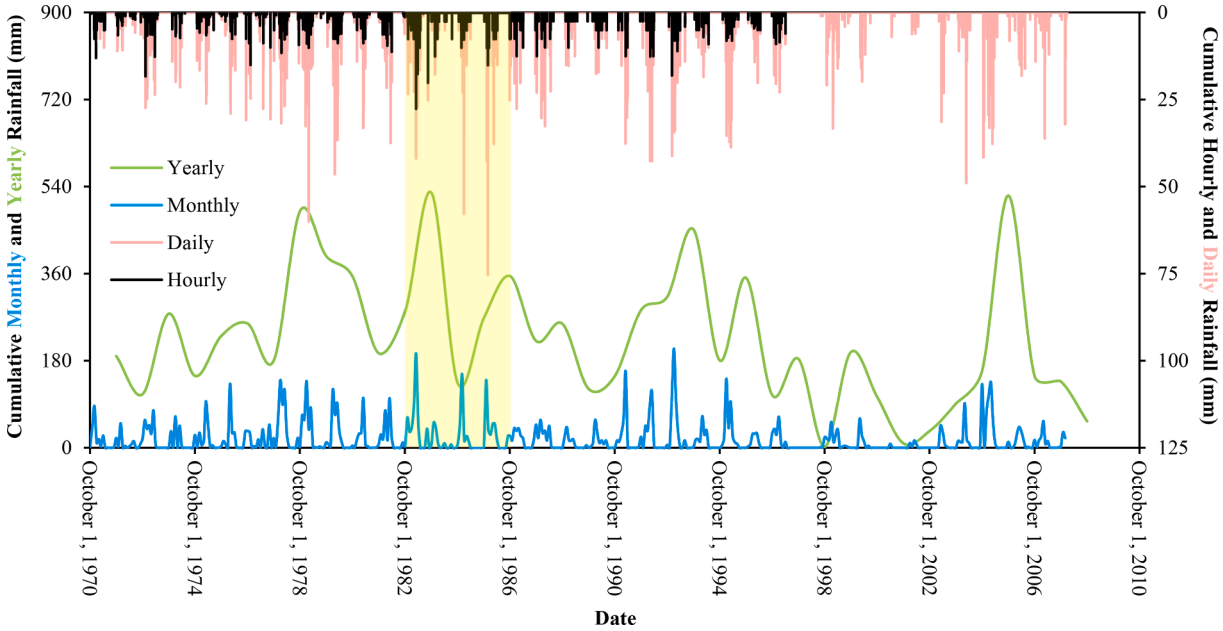

Fig. 3. Long-term rainfall data including the 4-year representative wet period (highlighted in yellow). (For interpretation of the references to colour in this figure legend, the reader is referred to the web version of this article.)

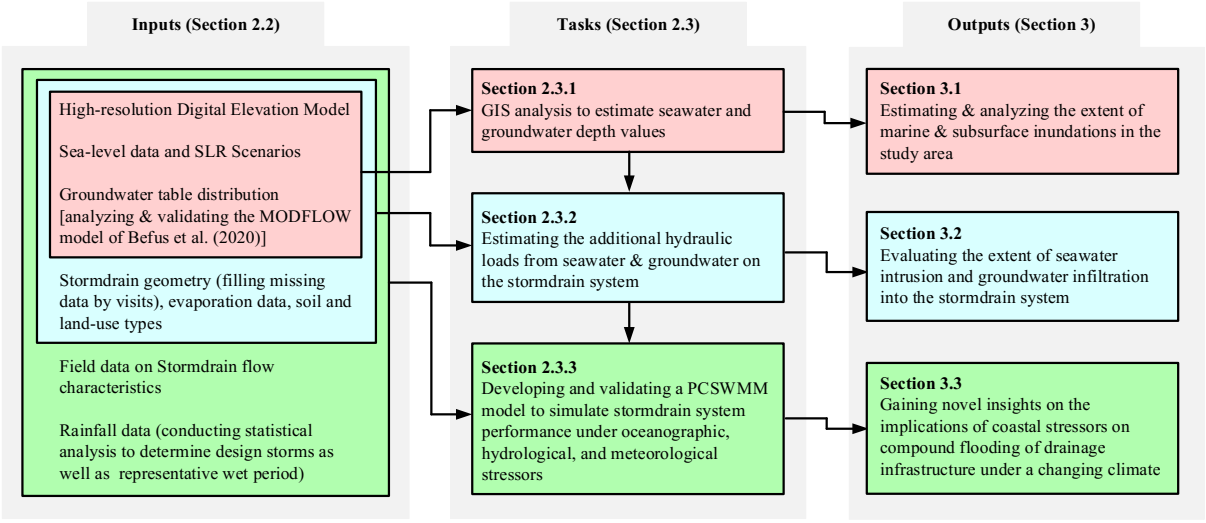

Fig. 4. Schematic diagram of the workflow carried out in the present study.

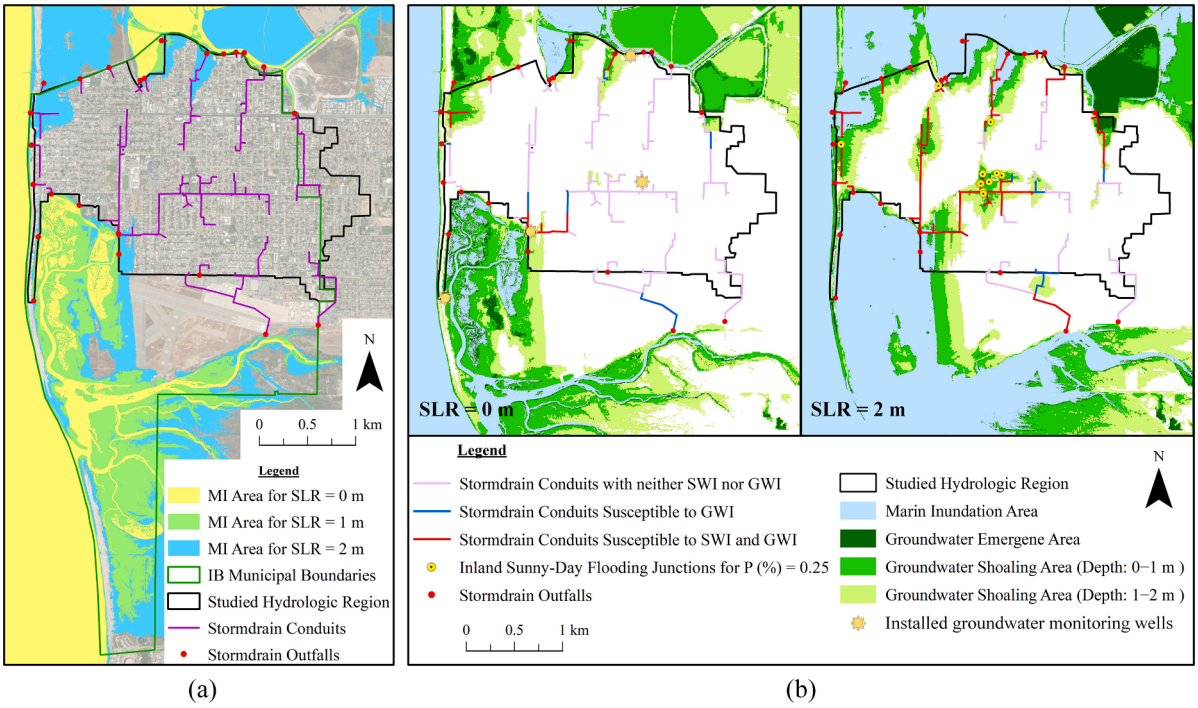

Fig. 5. Variations of (a) marine inundation and (b) groundwater emergence and shoaling for various SLR scenarios.

the identified areas without a surficial connection to the marine source are excluded from MI although the subsurface inundation still threatens these areas by flooding from underneath (Rotzoll and Fletcher, 2013). Through subtracting GWT elevation from the DEM, a similar method is applied to identify the areas potentially vulnerable to groundwater emergence and shoaling [as shown in Fig. 5(b) and described in section 3.1].

2.3.2. *Seawater intrusion and groundwater infiltration*

Flow conveyed through the stormwater network ultimately discharges through the outfalls (represented by red-filled circles in Fig. 5). By generating a reverse flow, SWI through the outfalls may limit the discharge capacity of the system at high sea-level conditions. This oceanographic stressor is considered in the stormdrain model simply by setting a fixed water elevation in the outfalls corresponding to the sea-level elevation for a given scenario. Generally, stormdrain system elements are susceptible to SWI if their elevations are lower than sea level.

As drainage pipes age, high-level groundwater may infiltrate into the system through the defects on the pipe walls and result in an increased hydraulic loading [see Fig. 6(a)]. Thus, in the case of having a defective system, stormdrain system elements are susceptible to GWI if their elevations are lower than local GWT. This study considers groundwater head (H_G) and system porosity (P) to estimate GWI rate into the stormdrain system. Considering the small variations of GWT (<5 cm changes over ~ 95 % of conduits), its average value above each conduit (GWT_{ave}) was used for GWI determination [see Fig. 6(b)]. Having a uniform value for the whole system, P is defined as the ratio of defect-to-conduit surface area in percent (results independency from defect position and size). Due to the lack of stormdrain monitoring data, three scenarios of $P = 0.000$, 0.125, and 0.250 % are defined in this study to

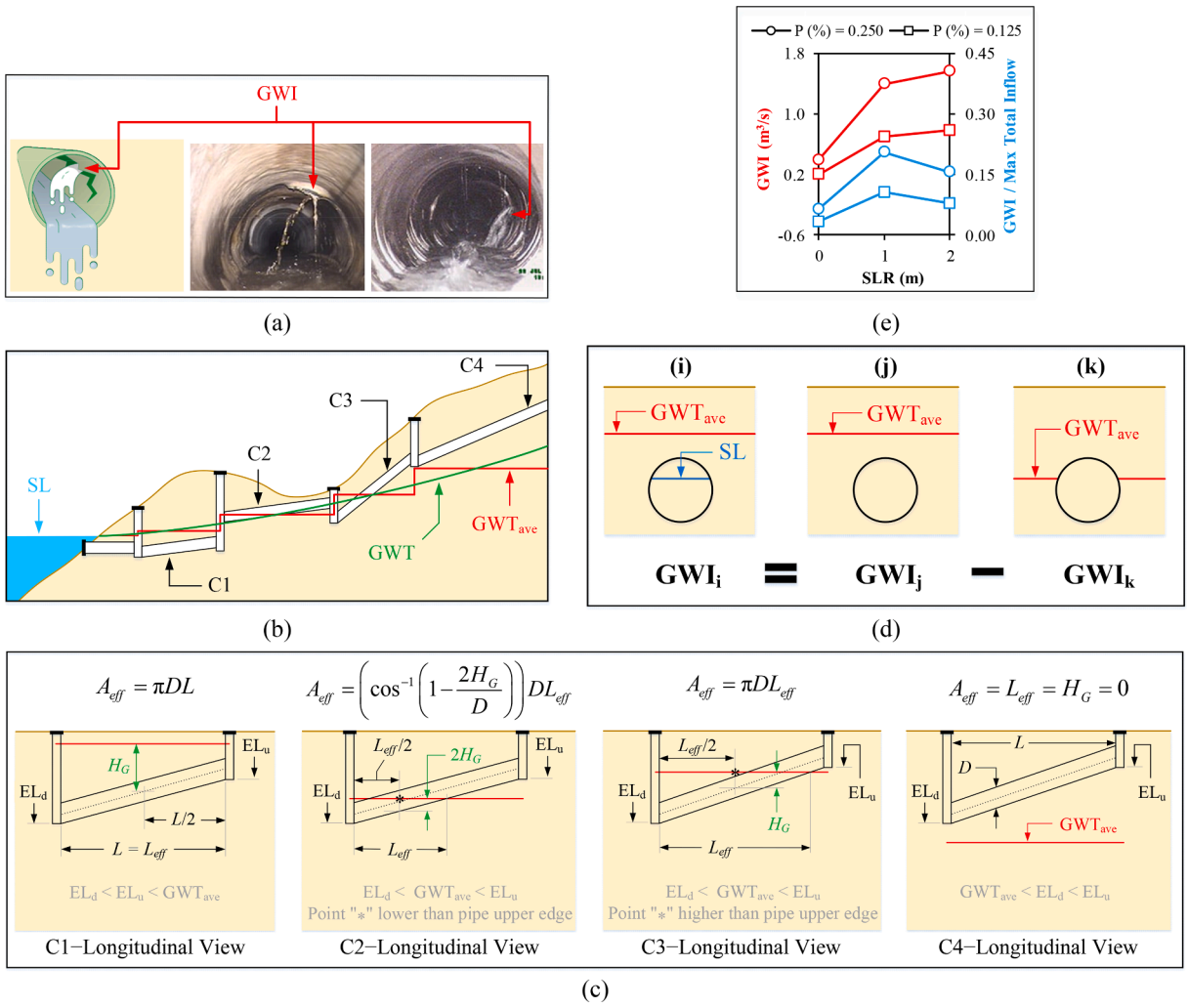

Fig. 6. Visualization of (a) GWI, (b) GWT and GWT_{ave} longitudinal profiles, (c) different GWT_{ave} situations with respect to conduits, (d) GWI determination in the presence of SWI, and (e) estimations of GWI into the system (normalized by the maximum total inflow during a 24-hr rainfall with 1-year return period).

evaluate the effects of system defects on its performance. Understanding the differences between stormwater and sewer networks, these scenarios are defined based on the CCTV sewer inspection dataset conducted in IB in 2014 (courtesy of the City of IB). To simplify the GWI calculation, non-circular conduits (consisting of < 5 % of total conduits) are approximated by equivalent circles $D = 4R$, where D and R are the equivalent circle diameter and the hydraulic radius of non-circular conduits, respectively.

The following assumptions are made to simplify the problem making it suitable for city-scale long-term simulations: (I) the surrounding soil is homogeneous and isotropic; (II) all system defects are in a regular circular form (in the order of cm) and uniformly distributed on the conduits (the results are independent of defect position and size); and (III) possible groundwater flow effects in terms of washing the surrounding soil can be neglected. Consequently, a modified form of the head-discharge equation for a circular orifice (Guo and Zhu, 2017) is used to determine the amount of GWI into the system,

$$\begin{aligned} GWI &= Q_d N = \frac{PA_{eff}}{25\pi}\varepsilon C_d\sqrt{gH_G} \\ Q_d &= \varepsilon C_d d^2\sqrt{gH_G} \\ N &= \frac{PA_{eff}}{100A_d} \end{aligned} \quad (1)$$

where Q_d = infiltration rate through a single defect; N = number of defects; ε = void ratio of the surrounding soil (=0.2); C_d = discharge coefficient of a circular orifice (=0.6); d = circular defect diameter; g = gravity acceleration; and A_{eff} = effective area for receiving GWI (=conduit surface area under GWT. As shown in Fig. 6(c), H_G and A_{eff} are estimated for each conduit based on its situation with respect to GWT_{ave} elevation. In addition, in the case of SWI into a conduit, the amount of GWI is determined through the presented superposition in Fig. 6(d). The calculated amount of GWI for each conduit is subsequently assigned as a constant flow rate to its upstream junction in the PCSWMM model.

2.3.3. Stormwater modeling

To simulate the stormdrain system performance, an integrated hydrology-hydraulic model is developed using PCSWMM (version 7.4.3240) with SWMM5 engine. To estimate surface runoff produced by rainfall over urban subcatchments, a nonlinear reservoir model is used along with Manning equation [Eqs. (2) and (3)]. Flow routing within conduits is governed by the conservation of mass and momentum [Eqs. (4) and (5) known as 1D Saint-Venant equations) (Rossman, 2015). The complete form of these equations (which refers to an unsteady and non-uniform flow in the system) is solved using the Finite Difference Method.

$$Change\ in\ depth\ over\ time = \frac{\partial d}{\partial t} = i - e - f - q \quad (2)$$

i = *rate of rainfall, snowmelt, and runon*; e = *evaporation rate*; f = *infiltration rate*; q = *runoff rate per unit surface area*.

$$q = \frac{Q}{A} = \frac{1}{n} R^{2/3} S_f{}^{1/2} \tag{3}$$

Q = *runoff volumetric flowrate*; A = *flow area* ($= W \times (d - d_s)$); n = *Manning roughness coefficient*; d_s = *depression storage*; W = *subcatchment width*; R = *hydraulic radius* ($= d - d_s$); S_f = *friction slope* [= *bed slope* (S_0) *in uniform flow*].

$$\frac{\partial Q}{\partial t} + \frac{\partial (Q^2/A)}{\partial x} + gA\frac{\partial H}{\partial x} + gAS_f = 0 \tag{4}$$

Q = *Volumetric flowrate* ($= A \times V$); A = *flow area*; V = *flow velocity*; H = *hydraulic head* ($= z + Y$); z = *elevation*; Y = *flow depth*; g = *gravity acceleration*.

$$\frac{\partial A}{\partial t} + \frac{\partial Q}{\partial x} = 0 \tag{5}$$

As shown in Fig. 7, the study area, consisting of 20 major drainage basins, is divided into 122 fine-resolution subcatchments to provide a precise rainfall-to-runoff modeling in the study area. In addition, the stormdrain system is described in a substantially high resolution by having 263 conduits in the model (linked to 200 open and 63 close junctions). Referring to the San Diego's Stormwater Standards (2017), the Green-Ampt method is selected for infiltration modeling while Manning roughness coefficients for subcatchments and conduits are determined in the ranges of 0.024–0.200 and 0.013–0.030, respectively. The energy loss coefficients at the entrance and exit conduits range from 0.1 − 1.0 based on their relative diameters to the neighboring junctions (Frost, 2006).

To calibrate and verify the model, wet-weather field monitoring data (courtesy of John Wood Group PLC) is obtained with a 1-min interval at the specified location in Fig. 7 (in the vicinity of IB's Public Library),

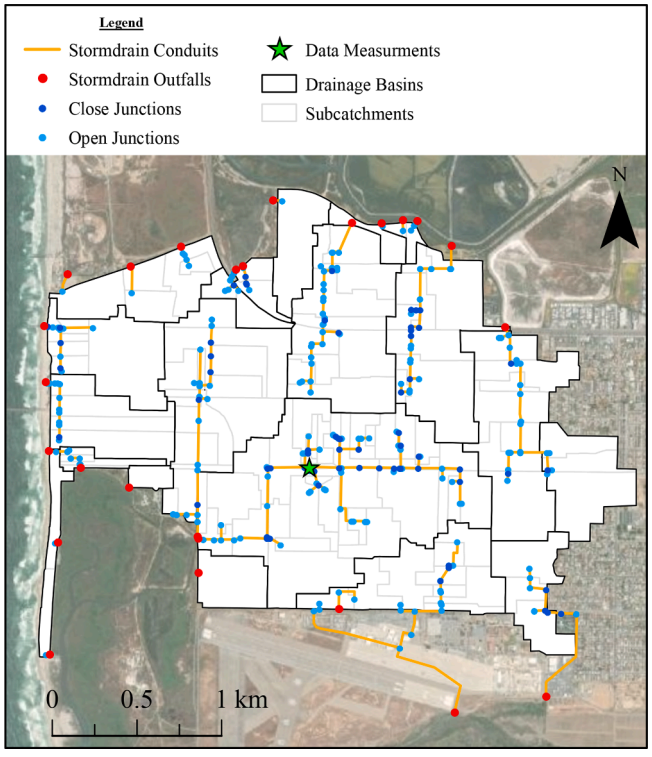

Fig. 7. Specifications of the PCSWMM stormwater model.

where the system is free of SWI and GWI in current conditions [see Fig. 5 (b)]. Satisfying the recommended ranges by the San Diego's Hydrology Manual (2003) for different land uses, the subcatchment imperviousness is set as the target parameter for calibration (ranging 25–80 %). According to Fig. 8, there is an outstanding agreement between the modeled and measured data for both calibration and verification periods. The modeled flow characteristics (i.e., stormdrain inflow and depth) match well with the measurements in terms of both the timing and magnitude of peak flow (<20 % difference).

Twenty scenarios are studied in this research (Table 3) to comprehensively evaluate the effects of SLR, system porosity, and rainfall properties on the performance of coastal stormdrain systems. According to Fischer et al. (2014), a ~ 25 % increase in heavy rainfalls could be expected in southern California by 2100. In Table 3, the nested storm with a 2-year return period corresponds to that increase in the intensity of the nested storm with a 1-year return period; thus, this magnitude of rainfall could be expected to happen every year (instead of every other year) in the region by the end of the century. However, no significant change in the annual mean precipitation is expected in the region (Fischer et al., 2014).

3. Results and discussion

3.1. Extent of marine and subsurface inundations

To improve the understanding of the vulnerability of coastal water infrastructure and resources to SLR, the first step is to assess the inundation potential. SLR-driven marine and subsurface inundation extents are shown in Fig. 5, and Table 4 summarizes the estimates of the impacted urbanized areas under no, moderate, and high SLR scenarios. The baseline year for the present-day condition (SLR = 0 m) scenarios is 2021.

From Fig. 2(a) and Fig. 5(a), Tijuana Estuary and its natural ecosystem will be extensively and directly impacted by marine inundation as sea level rises. However, marine inundation is predicted to have minimal impacts on the urbanized populated region where the present study focuses on. For SLR = 0, 1, 2 m scenarios, 0.00 %, 0.44 %, and 6.74 % of the urbanized area is under marine inundation, respectively (Table 4). The urban area inundation is limited to the San Diego Bay shoreline and the ocean facing coast (particularly along the thin strip between the ocean and estuary).

From Fig. 5(b) and Table 4, groundwater emergence and shoaling pose a more widespread threat than marine inundation for all SLR scenarios. In the current sea-level conditions, groundwater shoaling (with a depth < 2 m) threaten subsurface urban infrastructure in 8.5 % of the populated region (including areas far from the coastline). The SLR-induced groundwater rise will increase this number to 16.98 % and 23.01 % for 1 and 2 m SLR. Therefore, for the high SLR scenario, it is expected that around 30 % of the city will be permanently threatened by marine inundation and shallow GWT at the end of the century.

It is worth noting that both marine and subsurface inundations can be more widespread during dynamic ocean conditions (i.e., storm surge and wave action), which are excluded in the present study because of its focus on the long-term performance of the inland drainage system. In terms of spatial distribution, it is expected that the regions closer to the sea will be heavily impacted during dynamic sea-level events (Laster

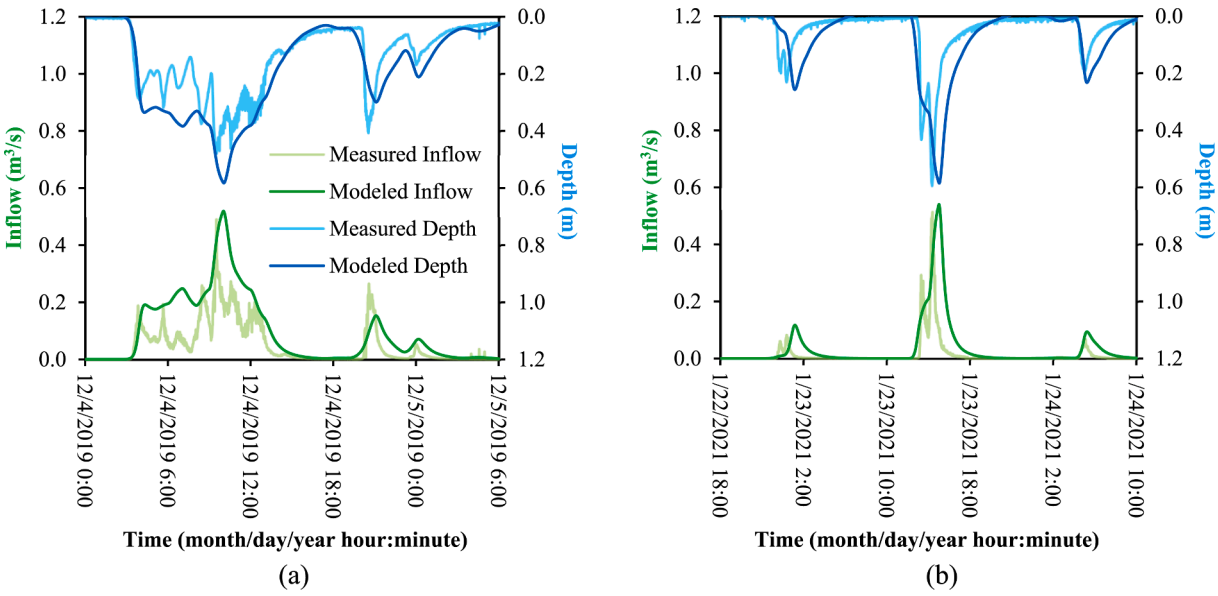

Fig. 8. Comparison of the measured and modeled data for (a) calibration and (b) verification periods.

Table 3
Studied scenarios in the present research.

Rainfall		SLR (m)	*P* (%)		
			0	0.125	0.250
24-Hour Nested Storm	1-Year Return Period	0	S0-P0.000-R1	S0-P0.125-R1	S0-P0.250-R1
		1	S1-P0.000-R1	S1-P0.125-R1	S1-P0.250-R1
		2	S2-P0.000-R1	S2-P0.125-R1	S2-P0.250-R1
	2-Year Return Period[I]	2	S2-P0.000-R2	S2-P0.125-R2	S2-P0.250-R2
	100-Year Return Period	0	S0-P0.000-R100	–	S0-P0.250-R100
		2	S2-P0.000-R100	–	S2-P0.250-R100
4-Year Historical Data		0	S0-P0.000-Historical	–	S0-P0.250-Historical
		2	S2-P0.000-Historical	–	S2-P0.250-Historical

[I] The nested storm with a 2-year return period corresponds to the 25% increase in the intensity of the nested storm with 1-year return period (happening every year in the region at the end of century).

Grip et al., 2021). From the studies of Gallien (2016) and Merrifield et al. (2021) on IB, the ocean shoreline will be particularly vulnerable to wave-driven impacts. Anderson et al. (2018) showed that the flooded area (mapped in three Hawaiian islands) can be increased up to 50 % by adding wave inundation to the passive flooding. In addition, a king tide can temporarily raise inland GWT while its fluctuations attenuate at a distance in the order of 1 km from the shoreline (Rotzoll and Fletcher, 2013).

3.2. Extent of seawater intrusion and groundwater infiltration

A substantial portion of the IB's stormdrain conduits is at risk of SWI and GWI through outfalls and system defects, respectively [Fig. 5(b)]. From Table 4, about 11 and 60 % of the conduits (with an invert elevation lower than sea level at MHHW) may experience some amount of SWI at the current and high sea-level conditions, respectively. In addition, the stormdrain conduits located in the emergent-to-shallow groundwater regions [Fig. 5(b)] are the most sensitive to GWI (enlarging by SLR-induced groundwater rise). At the high SLR scenario, ~67 % of the stormdrain length will be susceptible to GWI. This number is more than twice the above-mentioned percentage for the city area experiencing shallow GWT with a depth of<2 m (which is the typical depth for stormdrain systems). This difference is because a water drainage system with gravity-driven flow is typically located in low-lying regions of an urbanized area, where the risk of emergent-to-shallow groundwater is the highest. Therefore, water drainage systems are one of the most vulnerable coastal infrastructures to SLR impacts.

The estimations of GWI for different scenarios are plotted by the red-line graphs in Fig. 6(e). As expected, this parameter increases by rising sea level and spreading system defects. While it grows about four times by a 2 m SLR, GWI and *P* change with the same factor for a given sea level (due to assuming a uniform distribution of defects on the system).

Table 4
Percentages of the IB populated region (total area = 5,784,987 m^2) and the stormdrain system (total length = 15,961 m) impacted by marine and groundwater flooding sources.

SLR (m)	Marine Inundation Area (%)	Groundwater Emergence Area (%)	Groundwater Shoaling with <1 m Depth (%)	Groundwater Shoaling with <2 m Depth (%)	Length of Stormdrain Conduits susceptible to both SWI and GWI (%)	Length of Stormdrain Conduits susceptible to GWI (%)
0	0.00	0.02	2.18	8.50	11.09	20.10
1	0.44	1.51	7.17	16.98	38.26	41.11
2	6.74	0.62	9.53	23.01	60.00	66.73

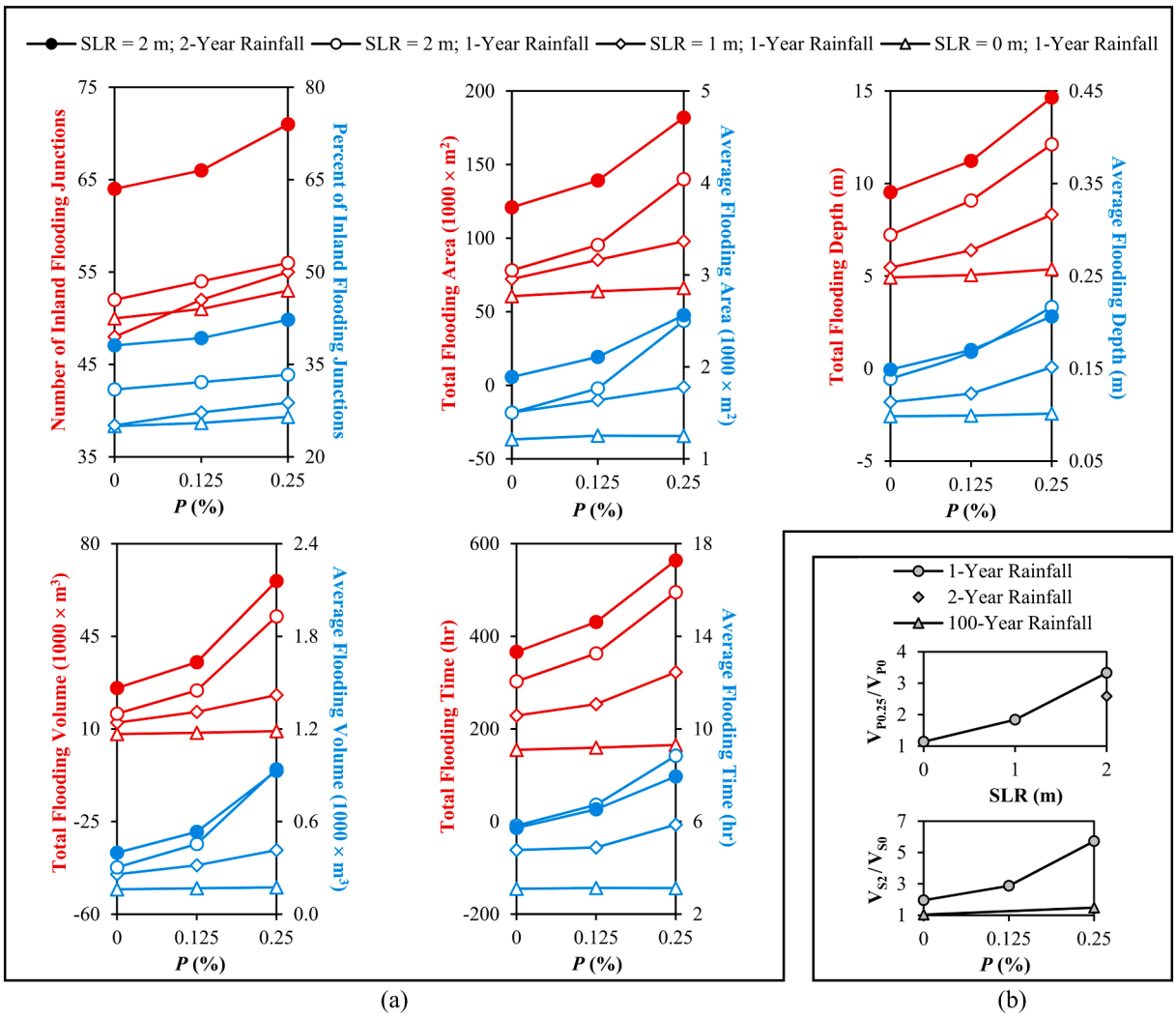

Fig. 9. Visualization of (a) main and (b) interaction effects of the studied parameters on compound flooding extent ($V_{P0.25}$, V_{P0}, V_{S2}, and V_{S0} on the vertical axes respectively refer to total flooding volume at P (%) = 0.25 & 0.00 and SLR = 2 & 0 m).

To have a better sense of the extent of this additional stressor, GWI is also normalized by the maximum total inflow during a 24-hr rainfall with a 1-year return period. As shown by the blue-line data in Fig. 6(e), GWI can consist of ~20 % of the maximum total inflow at SLR = 1 m. However, GWI may form a smaller part of the total inflow at higher SLR because of an increase in SWI contribution.

It should be noted that the SLR-induced groundwater lift in LECZs can cause some additional issues like exposing the public to sewage effluent contamination and degrading groundwater quality through saltwater intrusion into coastal aquifers (as shown in Fig. 1) and failure of immersed cesspool systems (Befus et al., 2020; Habel et al., 2020; Habel et al., 2017). These topics merit more research beyond the present study scope.

3.3. Compound flooding

The main effects of SLR, rainfall intensity, and stormdrain system porosity on its performance are presented in Fig. 9(a). As these parameters increase (which is expected to happen due to climate change effects and lack of maintenance in underserved areas), a higher percentage of inland junctions will flood (shown by the blue-line graphs in the top-left chart). The red-line graphs in other charts show that the stormdrain compound flooding is projected to increase in total area, depth, volume, and time over the century. We note that the junctions located in marine inundation areas are excluded from the stormdrain flooding analysis. This point may explain why the number of flooding junctions (shown by the red-line graphs in the top-left chart) is not a monotonic increasing function of SLR at $P = 0$. Unlike their total values, the average values of the flood properties (shown by the blue-line graphs in other charts) do not have a monotonic increasing trend with the rainfall return period. This is because although total flooding values increase during a 2-year rainfall event (more stormwater inflow), the increase in the number of flooding junctions may be larger; as a result, the average value may decrease (i.e., average value = total value / number of flooding junctions).

Interaction between different parameters implies that the effect produced by changing one parameter depends on the level of other parameters (Sangsefidi et al., 2017). Fig. 9(b) indicates the interactive effects of the three studied parameters on the total flooding volume (the vertical axis titles of the graphs are described in the figure caption). As shown, a more defective system will be impacted by SLR to a greater extent such that under a 1-year rainfall event, the flooding volume will grow up to 6 times by a 2 m rise in seal level when $P = 0.25$ %. However, this ratio may decrease to less than a third by avoiding GWI into the system ($P = 0$). Moreover, since the stormwater contribution to compound flooding increases by an increase in rainfall return period, the flooding extent is less sensitive to SWI and GWI under more extreme rainfall events.

No.	Location
❶	Date Ave at Seacoast Dr (W–E view)
❷	Intersection of Palm Ave and 2nd St (NE–SW view)
❸	Seacoast Dr at Carnation Ave (S–N view)
❹	Calla Ave at 5th St (S–N view)
❺	7th St at Delaware St (S–N view)
❻	8th St between IB Blvd and Elkwood Ave (E–W view)
❼	Ebony Ave at 11th St (W–E view)
❽	Intersection of 12th St and Holly Ave (SW–NE view)
❾	Oneonta Ave between 11th St and 12th St (W–E view)

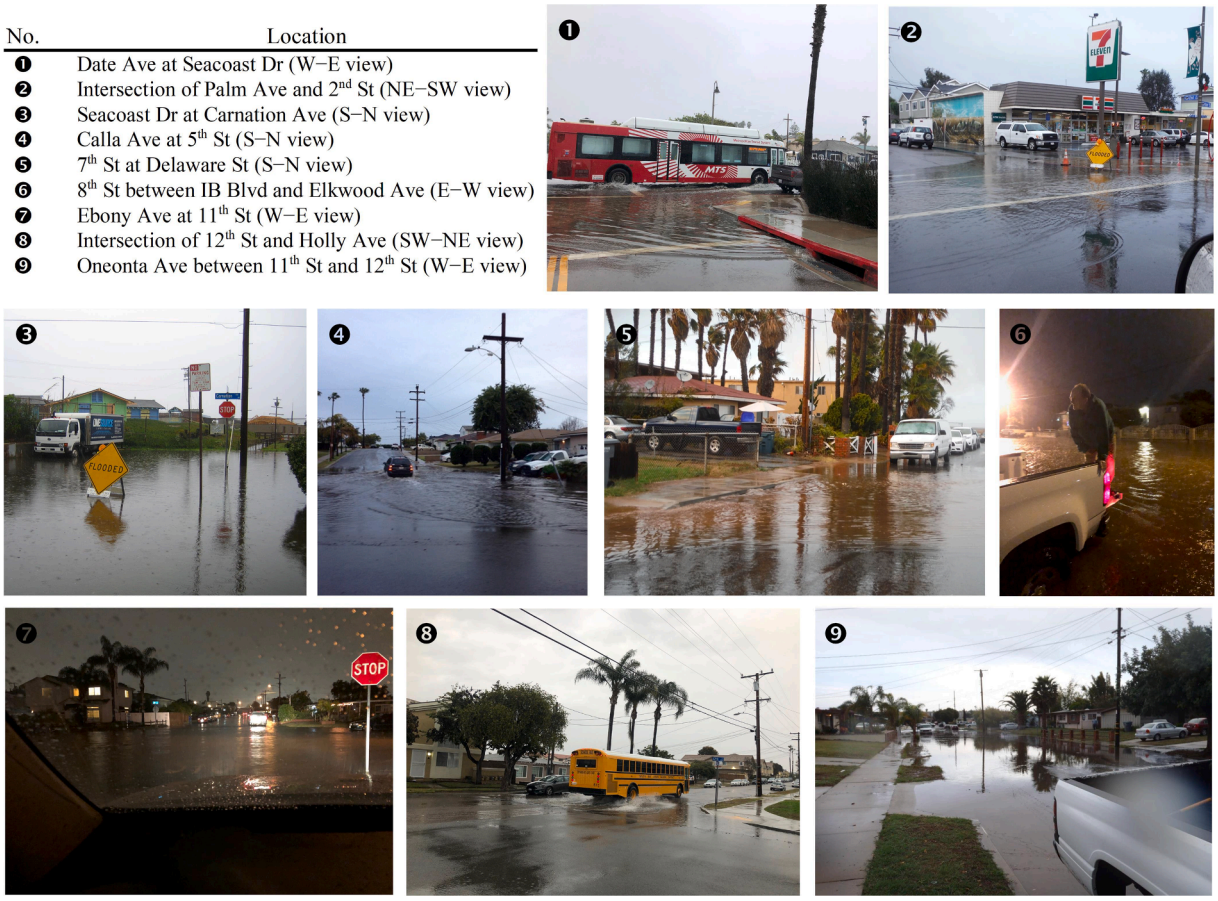

Fig. 10. Observations of the frequently flooded locations across The City of IB.

Fig. 10 shows today's observations of frequently flooded locations (courtesy of the City of IB), and Fig. 11 presents the flooding extent maps obtained from the developed stormwater model for five selective scenarios in current and future conditions (defined in Table 3). As a ground truth, Fig. 10 reveals that even for the current sea-level conditions, there are still serious problems across the city for draining stormwater from low-intensity rainfalls. This point also can be found from the presented flooding maps for S0-P0.000-R1 and S0-P0.250-R1 scenarios in Fig. 11, on which the nine frequently flooded locations are pinpointed. Considering the small extents of SWI and GWI at SLR = 0 m [Fig. 5(b)], the main driver of these floods should be rainfall-induced stormwater. From the comparisons of the two mentioned scenarios in Fig. 11, it can be found that the effects of system porosity are not significant in the current sea-level conditions (i.e., low GWT values in the region). By sea-level rising over the century, SWI may have a significant contribution in the stormdrain inflow and flooding (S2-P0.000-R1 scenario). However, comparison of the S2-P0.000-R1 and S2-P0.250-R1 scenarios indicates that the SLR impacts are considerably more severe for higher P values because GWI leads to a further increase in the hydraulic loadings on the system in these circumstances. As a result, the flooding hotspots during more-frequent design storms (i.e., 1-year return period) generally correspond to the shallow GWT regions depicted in Fig. 5(b).

Comparing the S0-P0.000-R1 and S2-P0.250-R1 scenarios (Fig. 11), the most important insight is that adverse impacts of SLR are not limited to marine inundation and a potential landward shift in the shoreline. SLR also can impact regions kilometers from the coastline through contributions to compound flooding events. The expected 25 % increase in the heavy rainfall intensities by climate change effects over the century (annual occurrence of the current 2-year rainfall in 2100) may cause additional stress on the system and enlarge the compound flooding extend even more (S2-P0.250-R2 scenario).

Based on the performed continuous simulations for the 4-year representative wet period, the long-term performance of the stormdrain system (as opposed to a single design storm) is analyzed by focusing on the selective junctions specified on the legend and bottom-left map in Fig. 11. As shown, the selected junction on each stormdrain line has a critical flooding condition compared to other junctions on that specific line. In addition, these junctions are selected from eight major stormdrain lines to inform us about various conditions of the system. Referring to Fig. 5(b), some selective junctions may be invulnerable to SWI and GWI while other ones can be susceptible to either SWI, GWI, or both. Fig. 12(a) presents the frequency (and number) of flood events with a separation time of 6 h. As shown, some parts of the system (i.e., K-629 and S-583 junctions) may experience similar flooding events in different scenarios because they receive neither SWI nor GWI [previously depicted in Fig. 5(b)]. However, for those parts susceptible to either SWI or GWI, the flood events are expected to happen more frequently depending on the amount of these additional stressors. For example, since junction #E-592 is at the risk of both SWI and GWI at SLR = 2 m, a higher number of flooding events is expected for this area compared to the current conditions [jumps in the data for S2-P0.000-Continuous and S2-P0.250-Continuous scenarios in Fig. 12(a)]. More challenging, some parts of the system may be always flooding at the end of the century (i.e., A-982, F-614, and H-610 junctions with a flood event frequency of 1) attributed to the high amount of SWI and GWI. Fig. 5(b) shows the 11 sunny-day flooding junctions across the study area for SLR = 2 m and P = 0.25 %, which are generally located in low-lying areas with emergent-to-shallow groundwater.

Fig. 12(b) demonstrates the flood frequency-volume plots for some of the selective junctions. As expected, larger floods happen less frequently in the region, and vice versa. Due to the contribution of SWI and GWI into stormdrain inflow, a flood with a given frequency will have a larger

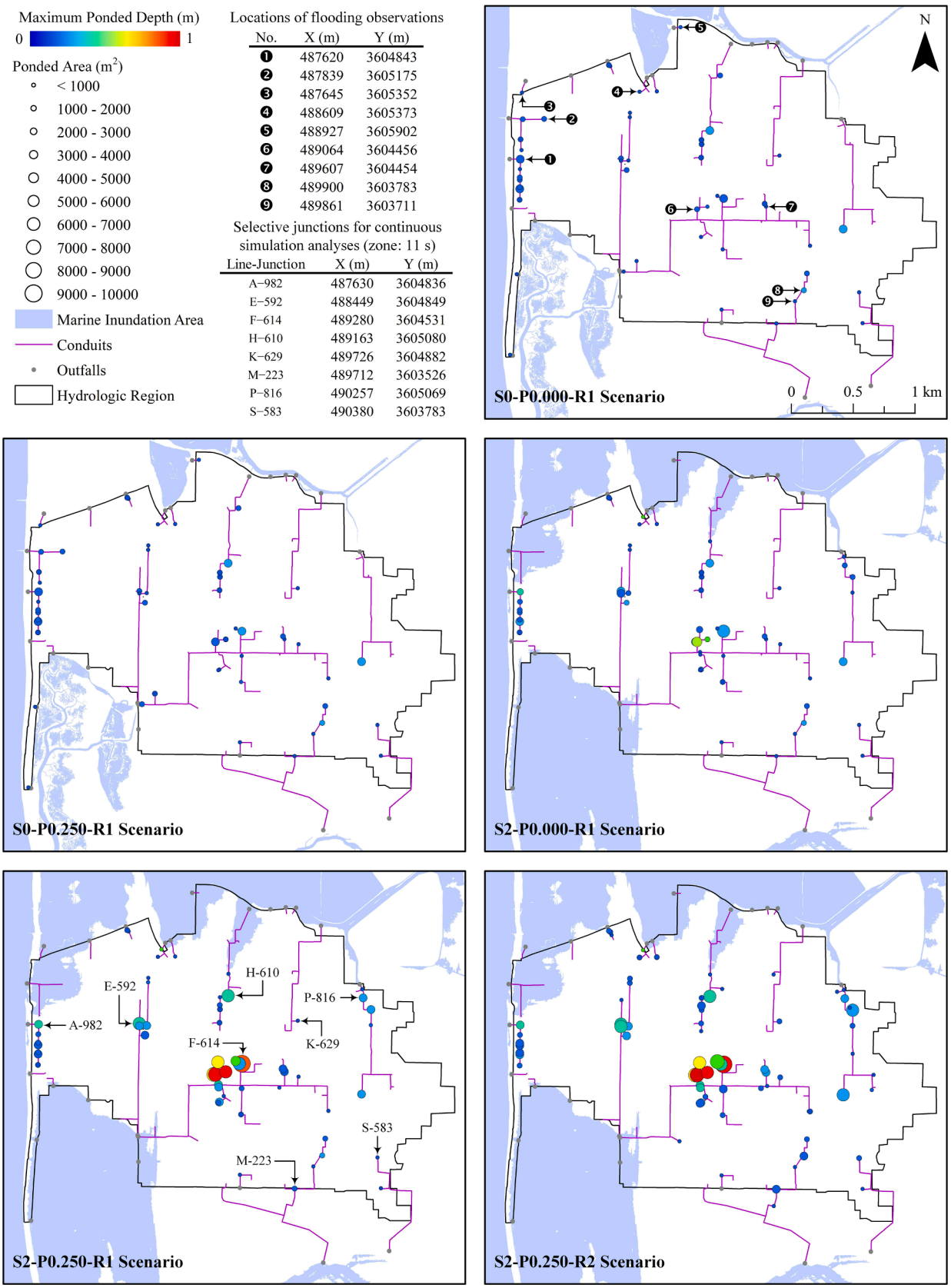

Fig. 11. Compound flooding maps for five selected scenarios (defined in Table 3).

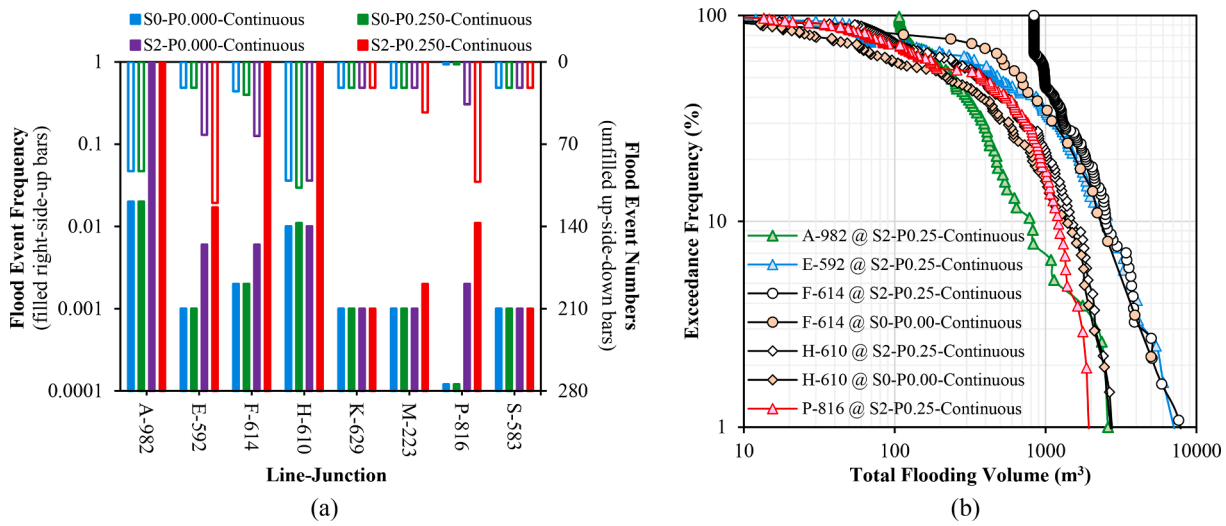

Fig. 12. Continuous simulation results for the specified junctions in Fig. 11: (a) flood event frequency and numbers (b) flood frequency-volume plot.

extent, or conversely, a given flood is expected to happen more frequently in the future. The effects of the SLR-induced stressors are more significant in more-frequent floods, especially in the sunny-day flooding areas. However, the difference between the data for S0-P0.000-Continuous and S2-P0.250-Continuous scenarios diminishes at lower values of flood frequency, and they eventually converge to each other for very extreme floods. In these circumstances, the contributions of seawater and groundwater sources in compound flooding are insignificant compared to that of the stormwater source. As a result, the flooding extent is highly dependent on the typical drainage characteristics of subcatchments (rather than SWI and GWI).

To improve our understanding of compound flooding extent and to develop adaptation strategies, we intend to pursue the following future research:

- Through installation of four groundwater wells inside Imperial Beach, the research team is collecting GWT data and estimating K in different areas of the city. These data will be utilized to develop a high-resolution 3D groundwater model to understand the spatial and temporal connection of sea-level events with groundwater flow (and contaminant transport).
- While rainfall is the main contributor to urban flooding in today's climate, storm waves may become the dominant stressor in the future, especially in downstream areas closer to the sea. In terms of temporal distribution, there also might be a shift in the dominant period from spring/autumn rain-induced flooding to winter sea-induced flooding due to energetic storm wave events originating in the North Pacific (Kunkel and Champion, 2019; Laster Grip et al., 2021). By adding storm wave action and local wind-driven surge to coastal stressors and including more site-specific conditions, a new 2D stormwater model will be developed and coupled with the groundwater model to determine emerging compound floodplains, which will be helpful for SLR mitigation and adaptation.
- Besides exposure to flood events, socioeconomic factors (e.g., race, income, public health, and education level), also should be taken into account for assessing the overall vulnerability of a community (Bathi and Das, 2016). In fact, identifying vulnerable population groups can be beneficial for prioritizing resources for underserved people. Through conducting extensive social studies and understanding the community barriers and motivations, adaption solutions will consist of environmentally-friendly engineered designs to protect the community against coastal climate change in a resilient and sustainable manner.

4. Conclusion and future works

This paper evaluates the vulnerability of the coastal stormdrain system at Imperial Beach to compound flooding of seawater, groundwater, and stormwater sources under climate change effects and possible impacts of lack maintenance due to resource limitations. The main conclusions are:

- Based on estimates of SLR-driven marine and subsurface inundations, we find that about two-thirds of the stormdrain length could be susceptible to SWI and GWI under the high SLR scenario of 2 m. In these conditions, GWI is estimated to increase up to 4 times and consist of twenty percent of the system hydraulic loads during annual rainfall events.
- With the contribution of SWI and GWI, the compound flooding extent will significantly increase in all forms of flooding depth, area, and time, and it can impact some areas kilometers away from the coastline. For a defective system (P = 0.25 %) working under a 1-year rainfall event, the flooding volume increases up to 6 times by a 2 m increase in current sea level. However, the flooding volume can be reduced to less than a third by repairing system defects and avoiding GWI into the system when SLR = 2 m.
- The oceanographic and hydrological stressors of SWI and GWI can also increase the frequency of flooding events in the region, while some low-lying areas with emergent-to-shallow groundwater may suffer sunny-day flooding.
- During extreme rainfall events (e.g., 100-year return period), the stormwater source dominates SWI and GWI, i.e., the system may fail solely by stormwater regardless of the other coastal stressors.

CRediT authorship contribution statement

Yousef Sangsefidi: Conceptualization, Methodology, Software, Validation, Formal analysis, Investigation, Data curation, Writing – original draft, Writing – review & editing, Visualization. **Kian Bagheri:** Methodology, Software, Writing – review & editing. **Hassan Davani:** Conceptualization, Methodology, Resources, Writing – review & editing, Supervision, Project administration, Funding acquisition. **Mark Merrifield:** Methodology, Resources, Writing – review & editing, Project administration, Funding acquisition.

Declaration of Competing Interest

The authors declare that they have no known competing financial

interests or personal relationships that could have appeared to influence the work reported in this paper.

Data availability

Data will be made available on request.

Acknowledgments

This research has been supported by the National Science Foundation under Grants No. 2113987 and 2113984. We appreciate the support of Computational Hydraulics Int. (CHI), The City of Imperial Beach (particularly Mr. Chris Helmer), and John Wood Group PLC for providing us with access to the PCSWMM license, stormdrain geometric data, and stormwater measurements, respectively.

References

Anderson, T.R., Fletcher, C.H., Barbee, M.M., Romine, B.M., Lemmo, S., Delevaux, J.M. S., 2018. Modeling multiple sea level rise stresses reveals up to twice the land at risk compared to strictly passive flooding methods. Sci. Rep. 8 (1), 14484.

Arkema, K.K., Guannel, G., Verutes, G., Wood, S.A., Guerry, A., Ruckelshaus, M., Kareiva, P., Lacayo, M., Silver, J.M., 2013. Coastal habitats shield people and property from sea-level rise and storms. Nat. Clim. Chang. 3 (10), 913–918.

Bathi, J., Das, H., 2016. Vulnerability of coastal communities from storm surge and flood disasters. Int. J. Environ. Res. Public Health 13 (2), 239.

Befus, K.M., Barnard, P.L., Hoover, D.J., Finzi Hart, J.A., Voss, C.I., 2020. Increasing threat of coastal groundwater hazards from sea-level rise in California. Nat. Clim. Chang. 10 (10), 946–952.

Bevacqua, E., Maraun, D., Vousdoukas, M.I., Voukouvalas, E., Vrac, M., Mentaschi, L., Widmann, M., 2019. Higher probability of compound flooding from precipitation and storm surge in Europe under anthropogenic climate change. Sci. Adv. 5 (9), eaaw5531.

County of San Diego Hydrology Manual (2003). <https://www.sandiegocounty.gov/content/dam/sdc/dpw/FLOOD_CONTROL/floodcontroldocuments/hydro-hydrologymanual.pdf>.

Davtalab, R., Mirchi, A., Harris, R.J., Troilo, M.X., Madani, K., 2020. Sea level rise effect on groundwater rise and stormwater retention pond reliability. Water 12 (4), 1129.

Dawson, R.J., Dickson, M.E., Nicholls, R.J., Hall, J.W., Walkden, M.J.A., Stansby, P.K., Mokrech, M., Richards, J., Zhou, J., Milligan, J., Jordan, A., Pearson, S., Rees, J., Bates, P.D., Koukoulas, S., Watkinson, A.R., 2009. Integrated analysis of risks of coastal flooding and cliff erosion under scenarios of long term change. Clim. Change 95 (1), 249–288.

Dirckx, G., Van Daele, S., Hellinck, N., 2016. Groundwater Infiltration Potential (GWIP) as an aid to determining the cause of dilution of waste water. J. Hydrol. 542, 474–486.

Fischer, E.M., Sedláček, J., Hawkins, E., Knutti, R., 2014. Models agree on forced response pattern of precipitation and temperature extremes. Geophys. Res. Lett. 41 (23), 8554–8562.

Frost, W.H., 2006. Minor loss coefficients for storm drain modeling with SWMM. J. Water Manage. Model. 517–546. R225-23.

Fung, A., Babcock, R., 2020. A flow-calibrated method to project groundwater infiltration into coastal sewers affected by sea level rise. Water 12 (7), 1934.

Gallien, T.W., 2016. Validated coastal flood modeling at Imperial Beach, California: Comparing total water level, empirical and numerical overtopping methodologies. Coast. Eng. 111, 95–104.

Gold, A.C., Brown, C.M., Thompson, S.P., Piehler, M.F., 2022. Inundation of stormwater infrastructure is common and increases risk of flooding in coastal urban areas along the US Atlantic Coast. Earth's Future 10 (3), e2021.

Guo, S., Zhu, D.Z., 2017. Soil and Groundwater Erosion Rates into a Sewer Pipe Crack. J. Hydraul. Eng. 143 (7), 06017008.

Habel, S., Fletcher, C.H., Rotzoll, K., El-Kadi, A.I., 2017. Development of a model to simulate groundwater inundation induced by sea-level rise and high tides in Honolulu, Hawaii. Water Res. 114, 122–134.

Habel, S., Fletcher, C.H., Anderson, T.R., Thompson, P.R., 2020. Sea-level rise induced multi-mechanism flooding and contribution to urban infrastructure failure. Sci. Rep. 10 (1), 3796.

Hauer, M.E., Evans, J.M., Mishra, D.R., 2016. Millions projected to be at risk from sea-level rise in the continental United States. Nat. Clim. Chang. 6 (7), 691–695.

Hoover, D.J., Odigie, K.O., Swarzenski, P.W., Barnard, P., 2017. Sea-level rise and coastal groundwater inundation and shoaling at select sites in California, USA. J. Hydrol.: Reg. Stud. 11, 234–249.

Jang, J.-H., Chang, T.-H., 2022. Flood risk estimation under the compound influence of rainfall and tide. J. Hydrol. 606, 127446.

Karamouz, M., Zahmatkesh, Z., Goharian, E., Nazif, S., 2015. Combined impact of inland and coastal floods: mapping knowledge base for development of planning strategies. J. Water Resour. Plan. Manag. 141 (8), 04014098.

Karpf, C., Krebs, P., 2011. Quantification of groundwater infiltration and surface water inflows in urban sewer networks based on a multiple model approach. Water Res. 45 (10), 3129–3136.

Khanam, M., Sofia, G., Koukoula, M., Lazin, R., Nikolopoulos, E.I., Shen, X., Anagnostou, E.N., 2021. Impact of compound flood event on coastal critical infrastructures considering current and future climate. Nat. Hazards Earth Syst. Sci. 21 (2), 587–605.

Kirezci, E., Young, I.R., Ranasinghe, R., Muis, S., Nicholls, R.J., Lincke, D., Hinkel, J., 2020. Projections of global-scale extreme sea levels and resulting episodic coastal flooding over the 21st Century. Sci. Rep. 10 (1), 11629.

Kopp, R.E., Kemp, A.C., Bittermann, K., Horton, B.P., Donnelly, J.P., Gehrels, W.R., Hay, C.C., Mitrovica, J.X., Morrow, E.D., Rahmstorf, S., 2016. Temperature-driven global sea-level variability in the Common Era. Proc. Natl. Acad. Sci. 113 (11), E1434–E1441.

Kunkel, K.E., Champion, S.M., 2019. An assessment of rainfall from hurricanes Harvey and Florence relative to other extremely wet storms in the United States. Geophys. Res. Lett. 46 (22), 13500–13506.

Langevin, C. D., Hughes, J. D., Banta, E. R., Niswonger, R. G., Panday, S., and Provost, A. M. (2017). *Documentation for the MODFLOW 6 Groundwater Flow Mode*, United States Geological Survey (USGS), Book 6, Chapter A55.

Laster Grip, I., Haghighatafshar, S., Aspegren, H., 2021. A methodology for the assessment of compound sea level and rainfall impact on urban drainage networks in a coastal city under climate change. City Environ. Inter. 12, 100074.

Liu, T., Ramirez-Marquez, J.E., Jagupilla, S.C., Prigiobbe, V., 2021. Combining a statistical model with machine learning to predict groundwater flooding (or infiltration) into sewer networks. J. Hydrol. 603, 126916.

Merrifield, M.A., Johnson, M., Guza, R.T., Fiedler, J.W., Young, A.P., Henderson, C.S., Lange, A.M.Z., O'Reilly, W.C., Ludka, B.C., Okihiro, M., Gallien, T., Pappas, K., Engeman, L., Behrens, J., Terrill, E., 2021. An early warning system for wave-driven coastal flooding at Imperial Beach, CA. Nat. Hazards 108 (3), 2591–2612.

Moftakhari, H., Schubert, J.E., AghaKouchak, A., Matthew, R.A., Sanders, B.F., 2019. Linking statistical and hydrodynamic modeling for compound flood hazard assessment in tidal channels and estuaries. Adv. Water Resour. 128, 28–38.

Moghimi, S., Myers, M., Pe'eri, S., Zhang, Y. J., Fei, Y. (2021). Forecasting compound floods in complex coastal regions. *Eos (102)*, <https://doi.org/10.1029/2021EO210604>.

Nicholls, R., 2011. Planning for the impacts of sea level rise. Oceanography 24 (2), 144–157.

Nicholls, R.J., Cazenave, A., 2010. Sea-level rise and its impact on coastal zones. Science 328 (5985), 1517–1520.

Rahimi, R., Tavakol-Davani, H., Graves, C., Gomez, A., Fazel Valipour, M., 2020. Compound inundation impacts of coastal climate change: sea-level rise, groundwater rise, and coastal precipitation. Water 12 (10), 2776.

Rossman, L. A. (2015). Storm Water Management Model User's Manual Version 5.1.

Rotzoll, K., Fletcher, C.H., 2013. Assessment of groundwater inundation as a consequence of sea-level rise. Nat. Clim. Chang. 3 (5), 477–481.

Saharia, A.M., Zhu, Z., Atkinson, J.F., 2021. Compound flooding from lake seiche and river flow in a freshwater coastal river. J. Hydrol. 603, 126969.

Sangsefidi, Y., Mehraein, M., Ghodsian, M., Motalebizadeh, M.R., 2017. Evaluation and analysis of flow over arced weirs using traditional and response surface methodologies. J. Hydraul. Eng. 143 (11), 04017048.

Su, X., Belvedere, P., Tosco, T., Prigiobbe, V., 2022. Studying the effect of sea level rise on nuisance flooding due to groundwater in a coastal urban area with aging infrastructure. Urban Clim. 43, 101164.

Sukop, M.C., Rogers, M., Guannel, G., Infanti, J.M., Hagemann, K., 2018. High temporal resolution modeling of the impact of rain, tides, and sea level rise on water table flooding in the Arch Creek basin, Miami-Dade County Florida USA. Sci. Total Environ. 616–617, 1668–1688.

Sweet, W. V., Hamlington, B. D., Kopp, R. E., Weaver, C. P., Barnard, P. L., Bekaert, D., Brooks, W., Craghan, M., Dusek, G., Frederikse, T., Garner, G., Genz, A. S., Krasting, J. P., Larour, E., Marcy, D., Marra, J. J., Obeysekera, J., Osler, M., Pendleton, M., Roman, D., Schmied, L., Veatch, W., White, K. D., and Zuzak, C. (2022). Global and Regional Sea Level Rise Scenarios for the United States: Updated Mean Projections and Extreme Water Level Probabilities Along U.S. Coastlines. *NOAA Technical Report NOS 01*, National Oceanic and Atmospheric Administration, National Ocean Service, Silver Spring.

Tahvildari, N., Abi Aad, M., Sahu, A., Shen, Y., Morsy, M., Murray-Tuite, P., Goodall Jonathan, L., Heaslip, K., Cetin, M., 2022. Quantification of compound flooding over roadway network during extreme events for planning emergency operations. nat. Hazard. Rev. 23 (2), 04021067.

The City of San Diego Stormwater Standards (2021). <https://www.sandiego.gov/sites/default/files/sws_manual_may_2021_update.pdf>.

Thompson, P.R., Widlansky, M.J., Hamlington, B.D., Merrifield, M.A., Marra, J.J., Mitchum, G.T., Sweet, W., 2021. Rapid increases and extreme months in projections of United States high-tide flooding. Nat. Clim. Chang. 11 (7), 584–590.

Trenberth, K.E., 2011. Changes in precipitation with climate change. Climate Res. 47 (1), 123–138.

Vitousek, S., Barnard, P.L., Fletcher, C.H., Frazer, N., Erikson, L., Storlazzi, C.D., 2017. Doubling of coastal flooding frequency within decades due to sea-level rise. Sci. Rep. 7 (1), 1399.

Wahl, T., Jain, S., Bender, J., Meyers, S.D., Luther, M.E., 2015. Increasing risk of compound flooding from storm surge and rainfall for major US cities. Nat. Clim. Chang. 5 (12), 1093–1097.

Zhao, Z., Yin, H., Xu, Z., Peng, J., Yu, Z., 2020. Pin-pointing groundwater infiltration into urban sewers using chemical tracer in conjunction with physically based optimization model. Water Res. 175, 115689.